**Technical Report 1673**
September 1994

# Characterization and Simulation of an Acoustic Source Moving Through an Oceanic Waveguide

Michael Reuter

Approved for public release; distribution is unlimited.

# EXECUTIVE SUMMARY

The processing of acoustic energy produced in an oceanic waveguide by a moving source in a near-field scenario is a challenging task statistically due to the nonstationarity of the data induced by the source motion. Many techniques of time series analysis require the estimation of at least second-order moments of the data received at a sensor or an array of sensors. The inherent assumption is made that statistically consistent estimates can be determined from sufficiently long segments of data. However, data of adequate length may not be available in the near-field scenario and so reliable estimates are difficult to obtain.

In the first part of this report, we introduce a statistical characterization of the moving source via a time-varying linear-systems interpretation that inherently accounts for source motion. This approach demonstrates how spectral coherence, which is indicative of temporally nonstationary data, is dependent on various environmental and source parameters. In the second part, we present a technique that uses this interpretation to simulate the acoustic time series received at a sensor or an array of sensors of arbitrary geometry due to an acoustic source moving through an oceanic waveguide. This simulation can be used to test how source motion affects the performance of signal and array processing algorithms. We further demonstrate the utility of this algorithm by comparing simulation results with experimental data.

# CONTENTS

EXECUTIVE SUMMARY . . . . . iii
1 INTRODUCTION . . . . . 1
1.1 PHYSICAL ASSUMPTIONS . . . . . 1
1.2 DOCUMENT OUTLINE . . . . . 1
2 ACOUSTIC FIELD OF A SINUSOIDAL MOVING SOURCE . . . . . 2
2.1 STATEMENT OF PROBLEM . . . . . 2
2.2 SOLUTION OF FIELD . . . . . 2
3 TIME-VARYING LINEAR SYSTEMS . . . . . 5
3.1 BIFREQUENCY ANALYSIS . . . . . 5
3.2 STOCHASTIC SOURCE . . . . . 6
3.3 MOVING-SOURCE INTERPRETATION . . . . . 7
3.3.1 Time-Varying Channel Impulse Response . . . . . 7
3.3.2 Modal Group Velocity . . . . . 8
3.3.3 Modal Time Delay . . . . . 9
4 MOVING-SOURCE SIMULATION . . . . . 10
4.1 COMPUTING THE BIFREQUENCY SYSTEM FUNCTION . . . . . 10
4.2 GENERATING TIME SERIES . . . . . 12
5 SIMULATION RESULTS . . . . . 14
5.1 EXPERIMENT DESCRIPTION . . . . . 14
5.2 DATA ANALYSIS . . . . . 15
6 CONCLUSIONS . . . . . 21
7 RECOMMENDATIONS . . . . . 22
8 REFERENCES . . . . . 23
APPENDIX. TIME-VARYING MODAL GROUP VELOCITY AND MODAL ARRIVAL TIME . . . . . 24

## FIGURES

1. Source–receiver track scenario . . . . . 2
2. Support of temporally windowed channel impulse response . . . . . 8

3. Support of impulse response for $\Delta\tau/\Delta t = 2$ . . . . . 10

4. Support of aliased impulse response . . . . . 11

5. The combination of two channel impulse response segments . . . . . 13

6. Schematic of the SwellEx2–Catalina Basin environment . . . . . 14

7. Sensor geometry and source track . . . . . 15

8. Experiment: 45-Hz tonal on sensor 1 . . . . . 16

9. Simulation: 45-Hz tonal on sensor 1 . . . . . 16

10 Experiment: 45-Hz tonal on sensor 2 . . . . . 17

11. Simulation: 45-Hz tonal on sensor 2 . . . . . 17

12. Experiment: 95-Hz tonal on sensor 1 . . . . . 18

13. Simulation: 95-Hz tonal on sensor 1 . . . . . 18

14. Experiment: 95-Hz tonal on sensor 2 . . . . . 19

15. Simulation: 95-Hz tonal on sensor 2 . . . . . 19

16. Experiment: 40- to 120-Hz band on sensor 1 . . . . . 20

17. Simulation: 40- to 120-Hz band on sensor 1 . . . . . 20

# 1 INTRODUCTION

Adaptive array processing techniques presently in use rely upon estimating at least second-order moments of time series received at an array of sensors or phones. Usually for frequency-domain algorithms, classical spectrum estimation methods are employed [1, 2] to estimate the auto- and cross-spectra of data received at the array of sensors. An inherent assumption made in these techniques is that the sensor data are wide-sense stationary and ergodic. In practice, one assumes "piecewise stationarity," i.e., that these statistics can be estimated from sufficiently long segments of data. Unfortunately for some practical applications, data segments of adequate length may not be available. For instance, this may be the case for a moving source whose trajectory is quickly changing with respect to an array of sensors or the propagation environment, such as in a near-field or shallow-water environment. Array processing performance in these situations is difficult to predict analytically since the statistical reliability of the moment or spectrum estimates is called into question.

Therefore we identified the need for an algorithm that simulates the time series received at a stationary array of arbitrary geometry resulting from a source which is moving through an oceanic waveguide. Because of the near-field scenario, in which the instantaneous source position may vary considerably over time with respect to an array, we believed it important to include Doppler effects. With this simulation, we can study and compare the performance of assorted array geometries and the associated signal processing algorithms under these nonstationary conditions. This capability is valuable because it will allow the Navy to access system performance in a realistic ocean environment without resorting to costly array deployment.

We accomplish this task by using a time-variant linear-systems interpretation of the analytical results reported by Hawker [3] for a sinusoidal source. With this interpretation, we extend the solution to a source of arbitrary energy or power spectrum shape. The problem then easily is discretized both temporally and spectrally using Fourier and linear-systems theory. A similar approach is described in [4].

## 1.1 PHYSICAL ASSUMPTIONS

We assume in this document that the acoustic propagation environment is range independent and cylindrically symmetric and that it can be modeled adequately as a sum of discrete normal modes. If a continuous spectrum exists, it will be ignored.

## 1.2 DOCUMENT OUTLINE

In Section 2, we briefly review Hawker's results for the acoustic field of a sinusoidal moving source. In Section 3, we present time-varying linear-systems theory and interpret the results of Section 2 in this light. We then describe in Section 4 the discrete time and frequency simulation, and present some simulation results in Section 5. The conclusions and recommended future work are presented in Sections 6 and 7.

# 2 ACOUSTIC FIELD OF A SINUSOIDAL MOVING SOURCE

Several authors recently have demonstrated the utility of the analytical results presented by Hawker [3], particularly in the area of parameter estimation of sinusoidal sources [5, 6, 7]. In this section, we review Hawker's fundamental results and apply them to a broadband source. The equations we present here are conjugated versions of Hawker's, since the sinusoidal source we will use is of the form $e^{i\omega_o t}$ to agree with the traditional engineering definition of the forward Fourier transform.

## 2.1 STATEMENT OF PROBLEM

The moving-source problem involves finding the solution to the wave equation

$$\left(\nabla^2 - \frac{1}{c^2}\frac{\partial^2}{\partial t^2}\right)\psi = -\delta[\boldsymbol{r} - \boldsymbol{r}_{\mathbf{s}}'(t)]e^{i\omega_o t} \tag{1}$$

where ψ is the pressure due to a point source emanating from frequency $\omega_o$. The location vector $\mathbf{r}_{\mathbf{s}}'(t)$ of the source term on the right side of equation 1 now is dependent on time.

The simplifying assumption is made that the source has zero acceleration, moves with speed $\upsilon$, and remains at a constant depth. The schematic of the source–sensor geometry is shown in figure 1. Here $R(t)$ is the range of the source from the receiver and $\theta(t)$ represents the angle of the source with respect to the receiver as the source progresses along its track. $\theta(t)$ is zero at its closest point of arrival (CPA) and positive when the source moves beyond CPA.

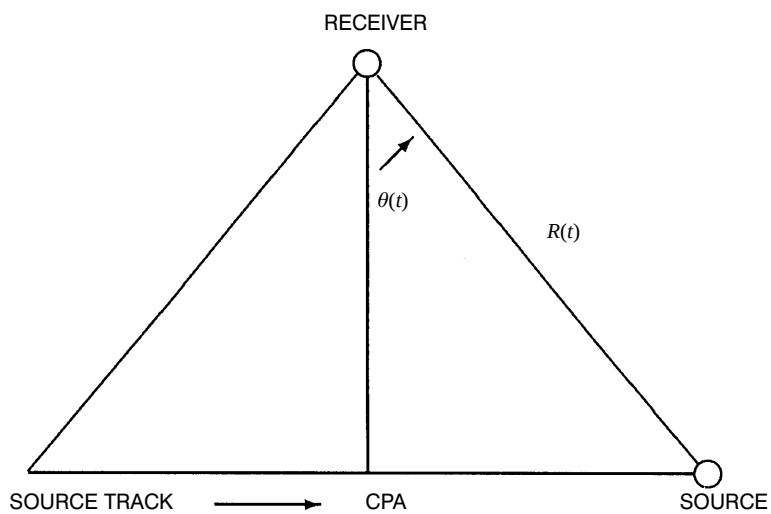


Figure 1. Source–receiver track scenario.

## 2.2 SOLUTION OF FIELD

Using the assumption that the acoustic propagation environment is range independent and cylindrically symmetric, Hawker [3] shows that the solution of equation 1 is approximately

$$\psi(t) = \frac{-1}{\sqrt{8\pi}} e^{i\omega_o t} e^{-i\pi/4} \sum_n \frac{Z_n(z_s)Z_n(z)}{\sqrt{k_n R(t)}} \exp\left[-ik_n R(t)\left(1 - \frac{\upsilon}{\upsilon_n^g}\sin\theta(t)\right)\right] \tag{2}$$

where

| | | |
|---|---|---|
| $Z_n$ | = | $n^{\text{th}}$ modal depth eigenfunction |
| $k_n$ | = | $n^{\text{th}}$ modal eigenvalue |
| $v_n^g$ | = | $n^{\text{th}}$ modal group velocity |
| $\alpha_n$ | = | $n^{\text{th}}$ modal attenuation term |
| $v$ | = | source speed |
| $z_s$ | = | source depth |
| $R(t)$ | = | time-dependent range |
| $\theta(t)$ | = | time-dependent angle. |

The modal values are all evaluated at the source frequency $\omega_o$. Equation 2 is valid under the additional condition that $v/v_n^g \ll 1$. As in [6], we have included an attenuation term in equation 2. Also note that equation 2 reduces to the well-known solution for the field of a stationary source by setting $v = 0$.

Now if we are interested in the field of the source around some arbitrary time $t_o$, we can expand $R(t)$ and $\sin\theta(t)$ about $t_o$ and apply the expansions to equation 2. Equation 2 can then be simplified by assuming that the source is moving sufficiently slowly so that the linear terms of the expansions are valid approximations of $R(t)$ and $\sin\theta(t)$ within a region of time $\Delta t$:

$$R(t) \approx R(t_o) + (t - t_o)R'(t_o)$$
$$\text{and} \tag{3}$$
$$\sin\theta(t) \approx \sin\theta(t_o) + (t - t_o)\theta'(t_o)\cos\theta(t_o)$$

Referring to figure 1, we get $R'(t_o) = v\sin\theta(t_o)$ and $\theta'(t_o) = v/R(t_o)\cos\theta(t_o)$. Then, ignoring the time dependence of $R(t)$ in the radical of equation 2, we can approximate $\psi(t)$ by

$$\psi(t) = \frac{-1}{\sqrt{8\pi}} e^{i\omega_o t} e^{-i\pi/4} \sum_n \frac{Z_n(z_s)Z_n(z)}{\sqrt{k_n R_o}} \exp\left[-ik_n R_o\left(1 - \frac{v}{v_n^g}\sin\theta_o\right)\right] \tag{4}$$
$$\exp\left[-iA_n(t - t_o)\right] e^{-\alpha_n R_o},\ t_o + M_D - \frac{\Delta t}{2} < t < t_o + M_D + \frac{\Delta t}{2}$$

where

| | | |
|---|---|---|
| $R_o$ | = | $R(t_o)$ |
| $\theta_o$ | = | $\theta(t_o)$ |
| $A_n$ | = | $k_n v\sin\theta_o - k_n v^2/v_n^g$ |

$M_D$ is the delay associated with the first modal arrival time associated with range $R_o$.

The approximation of equation 4 allows us to compute its Fourier transform analytically. The Fourier transform of length $\Delta t$ about $t_o + M_D$ of equation 4 is

$$\Gamma(\omega_o, u) = \frac{\Delta t}{\sqrt{8\pi}} e^{-i(u-\omega_o)t_o} e^{-i\pi/4} \sum_n \frac{Z_n(z_s)Z_n(z)}{\sqrt{k_n R_o}} \exp\left[-ik_n R_o\left(1 - \frac{v}{v_n^g}\sin\theta_o\right)\right] \tag{5}$$
$$\operatorname{sinc}(\nu_n \Delta t/2) e^{-\alpha_n R_o} e^{-i(A_n - \omega_o)M_D}$$

where

$$\nu_n = u - \omega_o + A_n$$

Equation 5 becomes invalid when the source is near CPA (small $|\theta_o|$), since in this region the linear terms used in the approximations of $R(t)$ and $\sin\theta(t)$ are not adequate. However, this is not a serious restriction, since in this region we can approximate the field of the moving source with that of a stationary one. Also, the condition that $v/v_n^g \ll 1$ is carried over to equation 5. The exponential term involving $M_D$ in equation 5 ensures that the transformed data are due to a source located about $R_o$.

Equations 4 and 5 demonstrate that we can interpret $A_n$ as the *modal Doppler shift*. The majority of the energy density spectrum of $\psi(t)$ due to the $n^{\text{th}}$ mode is concentrated about $u = \omega_o - A_n$. It is intuitively pleasing to see that for $v = 0$, $A_n = 0$, and there is no Doppler shift. Moreover, referring to figure 1, for $\theta_o > 0$, there is a negative shift in frequency for sufficiently large $\theta_o$, and for $\theta_o < 0$, there is a positive shift in frequency.

# 3 TIME-VARYING LINEAR SYSTEMS

The analysis of linear, time-varying continuous systems via the frequency domain was done some time ago by Zadeh [8]. More recently frequency-domain techniques have been applied to shift-variant discrete-time systems [9] and to time-varying filtering [10]. In this section, we review basic time-varying, linear-systems theory and use it to interpret the results of section 2.

## 3.1 BIFREQUENCY ANALYSIS

The output of a stable linear system is given by

$$y(t) = \int x(\tau)h(t,\tau)d\tau \tag{6}$$

where $h(t,\tau)$ is the system impulse response. Applying a complex sinusoidal input $x(t) = e^{i\omega t}$ and defining the *system function* [8] as

$$H(\omega;t) = e^{-i\omega t}\int h(t,\tau)e^{i\omega\tau}d\tau \tag{7}$$

we get

$$y(t) = H(\omega;t)e^{i\omega t} \tag{8}$$

$H(\omega;t)$ acts as a modulating signal of $e^{i\omega t}$. Equation 8 is identical in form to the time-invariant case except for the time dependence of $H(\omega;t)$.

The *bifrequency system function* $\Gamma(\omega,u)$ [8] is defined as the Fourier transform of the system response to $e^{i\omega t}$. Using equation 8 with the frequency variable $u$, we get

$$\Gamma(\omega,u) = \int H(\omega;t)e^{i(\omega-u)t}dt \tag{9}$$

Using equations 7 and 9, we can derive the inverse relations

$$H(\omega;t) = \frac{e^{-i\omega t}}{2\pi}\int \Gamma(\omega,u)e^{iut}du \tag{10}$$

$$h(t,\tau) = \frac{1}{2\pi}\int H(\omega;t)e^{-i\omega(\tau-t)}d\omega \tag{11}$$

and

$$h(t,\tau) = \frac{1}{4\pi^2}\int\int \Gamma(\omega,u)e^{iut}e^{-i\omega\tau}dud\omega \tag{12}$$

Using equation 12, we can see that $h(t, -\tau)$ and $\Gamma(\omega,u)$ form a two-dimensional Fourier transform pair:

$$h(t, -\tau) \overset{\mathcal{F}}{\Leftrightarrow} \Gamma(\omega, u) \tag{13}$$

Using equations 6 and 12, we get the Fourier transform of the output in terms of the bifrequency system function as

$$Y(u) = \frac{1}{2\pi} \int \Gamma(\omega, u) X(\omega) d\omega \tag{14}$$

where $X(\omega)$ is the Fourier transform of the input $x(t)$.

The following time-shifting relation, which is derived using equation 7, will be useful later. Defining $g(t,\tau) = h(t + \mu, \tau - \varepsilon)$, we get

$$G(\omega; t) = H(\omega; t + \mu) e^{i\omega(\mu + \epsilon)} \tag{15}$$

### 3.2 STOCHASTIC SOURCE

We now derive a basic relationship between the bifrequency system function and the spectral coherence function of the outputs of real, stable systems driven by a wide-sense stationary (WSS) stochastic source. The spectral coherence function displays the spectral correlation structure of a stochastic process [11] and is useful in the analysis of nonstationary processes.

Let $y_1(t)$ and $y_2(t)$ be the outputs of two real, stable linear systems driven by the same real, WSS process x(t):

$$\begin{aligned} y_1(t) &= \int x(\xi) h_1(t, \xi) d\xi \\ y_2(t) &= \int x(\eta) h_2(t, \eta) d\eta \end{aligned} \tag{16}$$

The cross-correlation function between $y_1(t)$ and $y_2(t)$ is then

$$R_{12}(t, s) = \int \int R_x(\xi - \eta) h_1(t, \xi) h_2(s, \eta) d\xi d\eta \tag{17}$$

Letting $S_x(\omega)$ be the power spectral density of the process x(t), and after exchanging the order of integration, we get

$$R_{12}(t, s) = \frac{1}{2\pi} \int \int \int S_x(\omega) e^{i\omega(\xi - \eta)} h_1(t, \xi) h_2(s, \eta) d\xi d\eta d\omega \tag{18}$$

Successive uses of equation 7 gives us

$$R_{12}(t, s) = \frac{1}{2\pi} \int S_x(\omega) H_1(\omega; t) H_2^*(\omega; s) e^{i\omega(t - s)} d\omega \tag{19}$$

Defining the spectral coherence function of $y_1(t)$ and $y_2(t)$ as [11]

$$S_{12}(\alpha,\beta) = \int\int R_{12}(t,s)e^{-i(\alpha t-\beta s)}dtds \tag{20}$$

and using equation 9, we finally get

$$S_{12}(\alpha,\beta) = \frac{1}{2\pi}\int S_x(\omega)\Gamma_1(\omega,\alpha)\Gamma_2^*(\omega,\beta)d\omega \tag{21}$$

If the two linear systems were time invariant, we would get

$$\begin{aligned}\Gamma_1(\omega,\alpha) &= 2\pi H_1(\omega)\delta(\omega-\alpha)\\ \Gamma_2^*(\omega,\beta) &= 2\pi H_2^*(\omega)\delta(\beta-\omega)\end{aligned} \tag{22}$$

where $\delta(\omega)$ is the Dirac delta function. Then, evaluating the convolution of delta functions [12], equation 21 reduces to

$$S_{12}(\alpha,\beta) = 2\pi S_x(\beta)H_1(\beta)H_2^*(\beta)\delta(\beta-\alpha) \tag{23}$$

Since in this case $y_1(t)$ and $y_2(t)$ are *jointly* WSS, we expect no correlation between different frequencies. This is demonstrated by equation 23, where the support of $S_{12}(\alpha,\beta)$ is only on the $\alpha = \beta$ portion of the bifrequency plane.

### 3.3 MOVING-SOURCE INTERPRETATION

We now present an interesting interpretation of the sinusoidal moving-source results of section 2 in terms of time-varying linear-systems theory. First, we recognize that the field generated by a sinusoidal source of equation 4 is simply the system function of equation 7 multiplied by $e^{i\omega t}$. Likewise the Fourier transform of the field of equation 5 can be viewed as the bifrequency system function of equation 9. Consequently, the inverse 2D Fourier transform of $\Gamma(\omega,u)$ generates the time-varying channel impulse response $h(t,\tau)$ (or equivalently the two-dimensional Greens function) for a particular geometry and source trajectory. Moreover, we can see from equations 5 and 21 how spectral coherence is dependent on the environmental and source parameters. We define the $t$ variable as *temporal response* and $\tau$ as *spatial time*. These terms are derived from the fact that the instantaneous location of the source is indexed by $\tau$, while the generated field time series received at a sensor is indexed by $t$.

#### 3.3.1 Time-Varying Channel Impulse Response

A physically realistic channel is causal. It also exhibits *finite* temporal response since we will assume some loss in the propagation environment. As a result, we can expect the time-varying channel impulse response to have support on the $(t,\tau)$ plane, as shown in figure 2. We can see that due to causality the support lies to the right of the $\tau = t$ line, i.e., for some spatial time $\tau_o$ we expect temporal response for $t > \tau_o$. Here the impulse response has been multiplied by a window of temporal width $\Delta t$ centered about $t_o$ with infinite spatial time length. We have eliminated the travel time $M_D$ of the lead pulse in the figure.

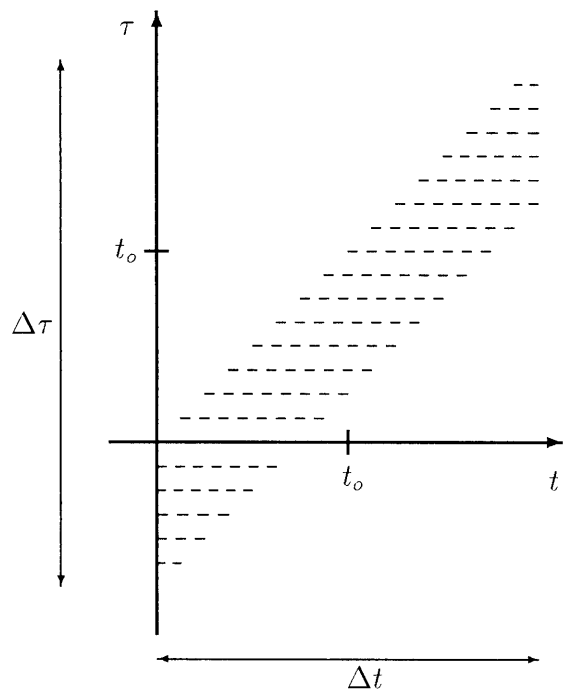


Figure 2. Support of temporally windowed channel impulse response.

### 3.3.2 Modal Group Velocity

In the appendix, we derive the time-varying modal group velocity using equation 11 and a stationary phase argument. The modal group velocity is shown to be

$$v^g_{n,\tau} = \frac{\left[R_o + v(\tau - t_o)\sin\theta_o\right]\left[1 - \frac{v}{v^g_n}\sin\theta_o + \left(\frac{v}{v^g_n}\right)^2 E_n\right]}{\frac{R_o}{v^g_n}\left[1 - \frac{v}{v^g_n}\sin\theta_o E_n\right] + (\tau - t_o)\left[\frac{v}{v^g_n}\sin\theta_o - \left(\frac{v}{v^g_n}\right)^2 E_n\right]} \tag{24}$$

for $-\frac{\Delta t}{2} + t_o < \tau < \frac{\Delta t}{2} + t_o$, where

$$E_n = \left(1 - k_n \frac{\partial v^g_n}{\partial \omega}\right) \tag{25}$$

We can see that $v^g_{n,\tau}$ differs from the stationary modal group velocity $v^g_n$. However, with $\tau = t_o$ (no expansion error in $R(t)$ and $\sin\theta(t)$) and assuming that $\left(\frac{v}{v^2_n}\right)^2 \ll 1$ and $E_n \approx 1$, we can see that $v^g_{n,\tau} \approx v^g_n$.

### 3.3.3 Modal Time Delay

Also in the appendix, we derive the modal arrival time as a function of spatial time. The modal delay is shown to be

$$M_{D,n} = \frac{\frac{R_o}{v_n^g}\left(1-\frac{v}{v_n^g}\sin\theta_o E_n\right) + (\tau - t_o)\left[\frac{v}{v_n^g}\sin\theta_o - \left(\frac{v}{v_n^g}\right)^2 E_n\right]}{\left[1-\frac{v}{v_n^g}\sin\theta_o + \left(\frac{v}{v_n^g}\right)^2 E_n\right]} \tag{26}$$

for $-\frac{\Delta t}{2} + t_o < \tau < \frac{\Delta t}{2} + t_o$.

Assuming that $\frac{\partial v_n^g}{\partial \omega} \approx 0$, $E_n \approx 1$, and $\left(\frac{v}{v_n^g}\right)^2 \approx 0$, we can approximate $M_{D,n}$ as

$$M_{D,n} \approx \frac{R_o}{v_n^g} + (\tau - t_o)\left(\frac{\frac{v}{v_n^g}\sin\theta_o}{1 - \frac{v}{v_n^g}\sin\theta_o}\right) \tag{27}$$

for $-\frac{\Delta t}{2} + t_o < \tau < \frac{\Delta t}{2} + t_o$.

We can see that the modal time delay is a linear function of $\tau$. In the approximation of equation 27 at $\tau = t_o$, we get the traditional modal time delay $R_o/v_n^g$ [13]. We can also see that for a trajectory in which the source approaches the receiver ($\theta_o < 0$), we get the physically intuitive result that $M_{D,n}$ is less than $R_o/v_n^g$ for $\tau > t_o$ and greater than $R_o/v_n^g$ for $\tau < t_o$. The situation is reversed when $\theta_o > 0$.

# 4 MOVING-SOURCE SIMULATION

The results presented in sections 2 and 3 represent the building blocks of an algorithm that simulates the time series received at a sensor from the acoustic energy emitted by a source moving through an oceanic waveguide. The technique essentially involves discretizing the integral in equation 14. We compute the bifrequency system functions for various spatial time and temporal response segments over the source track, use a discrete version of equation 14 to compute the frequency-domain representation of the sensor data for each segment, inverse transform, and then fit the pieces together appropriately. We describe the basic technique in this section.

## 4.1 COMPUTING THE BIFREQUENCY SYSTEM FUNCTION

Determining the spectral sampling resolution ($\Delta u$ and $\Delta\omega$) of the bifrequency system function of equations 5 and 14 is the most critical aspect of the simulation. The approach taken here utilizes the fundamental concepts of the 2D sampling theorem to obtain the appropriate resolution.

We will assume that the source process is strictly band limited so that we can spectrally window $\Gamma(\omega, u)$. Next, from the sampling theorem, we observe that $\Delta t = 2\pi/\Delta u$ and $\Delta\tau = 2\pi/\Delta\omega$. The spectral resolution will therefore determine the size of the 2D time window. In the implementation of the algorithm, we fix the ratio $\Delta\tau/\Delta t$ to 2 so that $\Delta u/\Delta\omega = 2$. The support of the resulting time-varying impulse response is shown in figure 3 with the initial bulk delay $M_D$ removed and with $t_o = \Delta t/2$.

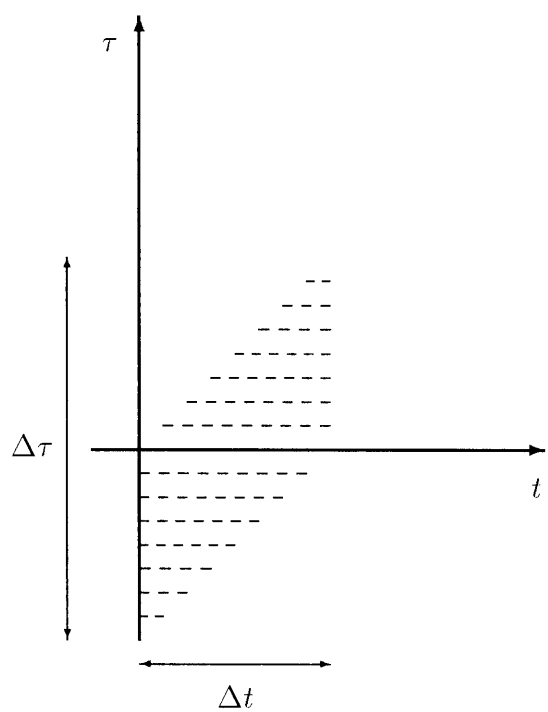


Figure 3. Support of impulse response for $\Delta\tau/\Delta t = 2$.

Now, we determine the adequate spectral resolutions simply by sampling $\Gamma(\omega,u)$ so that we minimize the distortion in the resulting sampled channel impulse response $h(n,m)$. While we never explicitly need to evaluate $h(n,m)$ in the algorithm, it is essential to sample $\Gamma(\omega,u)$ adequately since the technique has a time-domain interpretation which is a discrete version of equation 6:

$$y(n) = \sum_m x(m)h(n,m) \tag{28}$$

So we must minimize the distortion in $h(n,m)$ to maintain the fidelity of the sensor time series. We desire an $h(n,m)$ which has support similar to that of figure 3. Undersampling will result in the aliasing of $h(n,m)$ similar to that shown in figure 4, where we show only the first period. Moreover, if the maximum temporal response of the channel is greater than the $\Delta t$ determined by the spectral resolutions, $h(n,m)$ will also be aliased. As a result, we can see that the choice of $\Delta\tau/\Delta t = 2$ is the most conservative choice since the restriction on the impulse response is that the maximum temporal response (less the initial delay $M_D$) be less than or equal to $\Delta t$. Other values of $\Delta\tau/\Delta t$ will require the temporal response to be much shorter, i.e., $\frac{1}{2}\Delta t$, $\frac{1}{3}\Delta t$, etc.

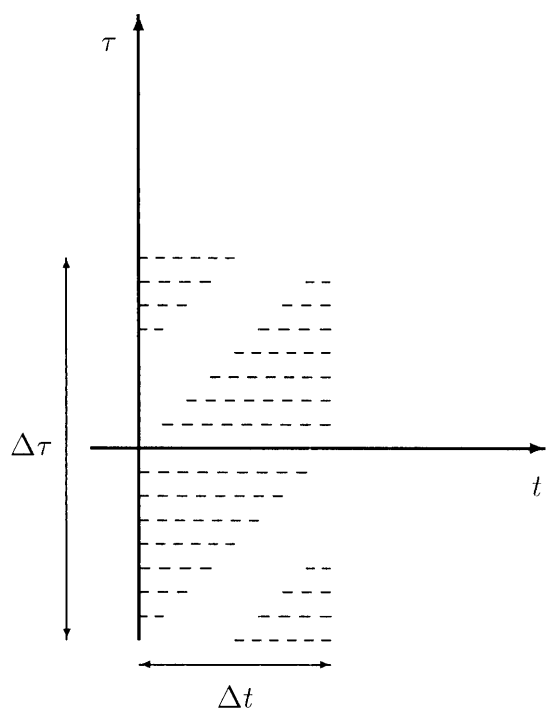


Figure 4. Support of aliased impulse response.

We previously removed the first modal arrival time $M_D$ from the channel impulse response $h(n,m)$ to reduce the spectral sampling resolution and thereby considerably reduce the computational burden. This task is easily accomplished in the frequency domain by using the time-shifting property of the system function of equation 15. We simply multiply $H(\omega;t)$, or equivalently $\Gamma(\omega,u)$, by $e^{i\omega M_{D,min}}$. We estimate $M_{D,min}$ by using equation 26 or 27 and eigenvalue and modal group velocity values at the center of the band. To account for the fact that the minimum arrival time $M_{D,min}$ is a linear function of $\tau$ with a slope that is a function of the source trajec-

tory, we apply the results of section 3.3.3 and use $\tau = 0$ if $\theta_o > 0$ and $\tau = \Delta t$ if $\theta_o < 0$. $t_o = \Delta t/2$ for both cases.

We must also account for the fact that the bifrequency system function of equation 5 derived in [3] is not a valid approximation near CPA. In the algorithm, we set $\upsilon = 0$ in equation 5 when –5 degrees < $\theta_o$ < 5 degrees and proceed as above where now $M_{D,\min} = R_o/\upsilon_n^g$.

## 4.2 GENERATING TIME SERIES

We generate the time series received at a sensor via the frequency domain by discretizing the integral in equation 14. Letting $T$ be the sample interval, we get $\Delta t = NT$ and $\Delta\tau = MT$, where $N$ and $M$ are the number of temporal response and spatial time samples in each segment. Then

$$Y(k) = \frac{1}{MT}\sum_l \Gamma(l\Delta\omega, k\Delta u)X(l) \tag{29}$$

where $X(l)$ is the discrete Fourier transform (DFT) of a section of time series emitted by the source of length $M$ samples, and $Y(k)$ is the DFT of the sensor time series of length $N$ samples. An inverse DFT of $Y(k)$ then produces the sensor time series $y(n)_{n=1}^{N}$. The source has arbitrary spectral as well as statistical characteristics. This technique is applicable to wide-sense stationary as well as nonstationary or transient sources.

Next we must combine the time series generated in each segment so that we create a seamless transition between spatial–temporal segments. We accomplish this by appropriately overlapping the *input* time series $x(n)$ from one segment to the next. If the source were stationary, we would use source data $x(n)$ the first half of which consists of old data emitted by the source in the previous segment, and the second half consists of new data. This is evident from equation 28 and an analysis of figure 5, where we display two contiguous segments evaluated at different source positions. We then join consecutively the sensor time series $y(n)$ from each segment. However, for a moving source, it is important that we account for the fact that the time-varying minimum modal arrival times $M_{D,min}$ induce an expansion or contraction in the output time series, depending on the source trajectory (sign on $\theta_o$). For instance, assume the source is moving away from the sensor ($\theta_o > 0$). When we left-shift the channel impulse response by $M_{D,min}$ evaluated at $\tau = 0$, we must allow for the fact that we will shift the immediately following segment by a *greater* amount due to the source trajectory and greater range for that segment. Conversely, if the source is approaching the sensor ($\theta_o < 0$), we left-shift the following segment by a *smaller* amount. When the source is moving away from the sensor, we define $D$ as the difference in samples between the left shift of the present segment and the previous segment. Then we use an additional $D$ old samples in the source time series data $x(n)$ in our calculation of $y(n)$. And when the source is approaching the sensor, we define $D$ as the difference in samples between the left shift of the previous segment and the present segment. Then we calculate $y(n)$, using $x(n)$ as in the stationary source case, except that we throw away the first $D$ samples of $y(n)$.

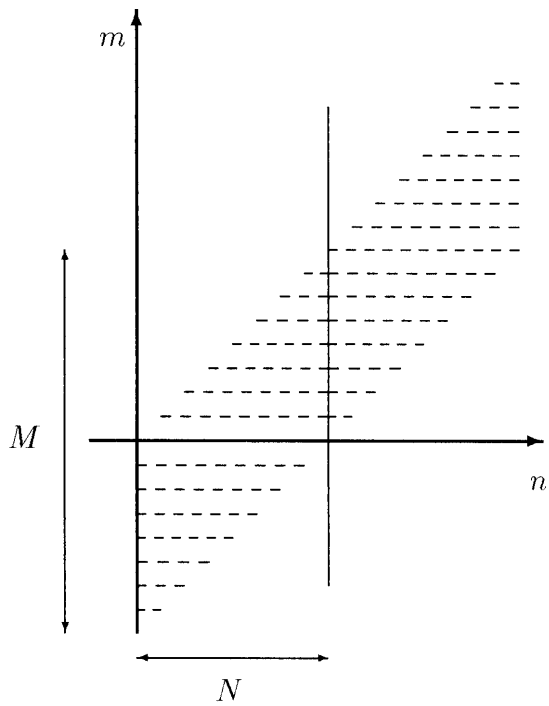


Figure 5. The combination of two channel impulse response segments.

Finally, we note that the bifrequency system function $\Gamma(\omega,u)$ of equation 5 has significant value only for regions of $u$ around $\omega - A_n$ due to the sinc function in the summation. To reduce the computational burden of calculating $\Gamma(\omega,u)$ over the entire frequency range of $u$, we can calculate $\Gamma(\omega,u)$ only for regions of $u$ where the sinc function has significant value, e.g., the first and second lobes. We set the remaining regions of $\Gamma(\omega,u)$ to zero. We call this modification *partial bifrequency calculation*. Caution must be used here since we introduce errors across the spectral band. We can then expect temporal distortions at the seams of the segments.

# 5 SIMULATION RESULTS

In this section, we demonstrate the capabilities of the algorithm by presenting some simulation results. As a measure of performance, we will compare simulated time series with data collected during the SwellEx2 experiment held September 1993 in the Catalina basin. A schematic of the environment of interest is shown in figure 6, which includes the depth-dependent sound speeds and the density and attenuation factors in the sediment layer and bottom half space.

We have incorporated the KRAKEN normal mode program [14] into the software to generate the eigenvalues and eigenfunctions.

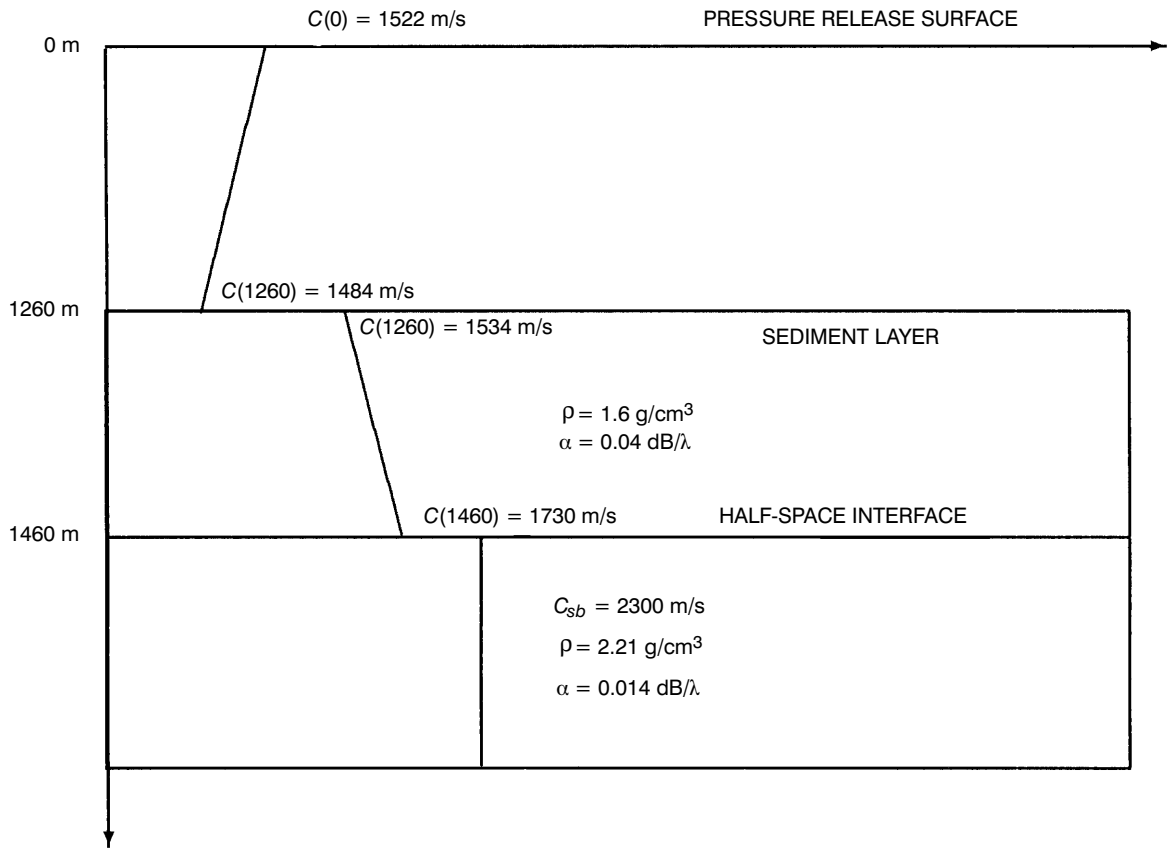


Figure 6. Schematic of the SwellEx2–Catalina Basin environment.

## 5.1 EXPERIMENT DESCRIPTION

The sensor and source track geometry used in this comparison are shown in figure 7. We will only use two sensors from the deployed array. An “X” marks the horizontal position of each bottom–mounted sensor. The data are sampled at 434.03 samples/s. A tug boat tows a source that is at a depth of 49 meters and is emitting 45- and 95-hertz tonals. The tug is at a nominal depth of 6 meters. We present results from 1 hour of experimental data in which the tug, moving at approximately 4 knots, passes between the two sensors at the 30-minute point, and the displayed trajectory, and compare these results with simulated data generated by using this environmental and source–sensor scenario.

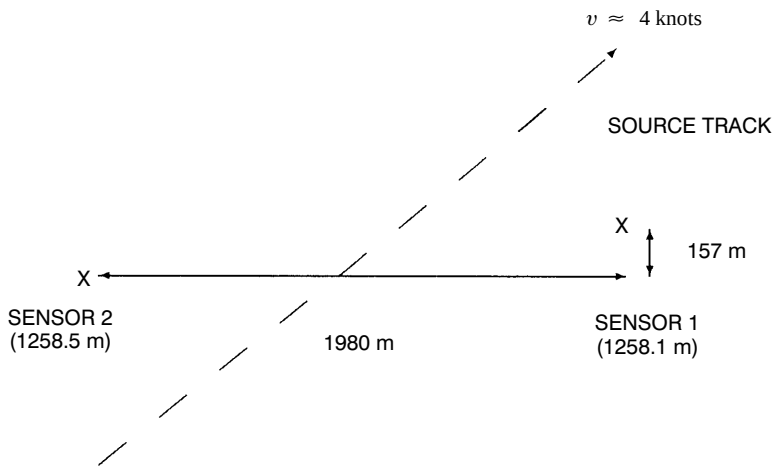


Figure 7. Sensor geometry and source track.

## 5.2 DATA ANALYSIS

Figure 8 is a spectrogram of sensor 1 centered about the 45-Hz tone of the experimental data set. Figure 9 is the spectrogram of the corresponding simulated data. The algorithm models a narrowband source as a second-order autoregressive process. This may account for the fuzzy nature of the line in figure 9. In both figures, the characteristic knee in the line at approximately the 35-minute mark indicates Doppler shift associated with a CPA event. Figures 10 and 11 are the corresponding spectrograms of sensor 2. As expected from the source trajectory plot of figure 7, the knee in the source line occurs earlier in the data, at approximately the 20-minute mark.

More dramatic Doppler effects are evident in figures 12 to 15, which are the spectrograms of sensors 1 and 2 centered at 95 Hz. Again the Doppler effects observed in the experimental data agree with those in the simulated data.

To demonstrate the effect of a moving broadband source, we model the tug as a broadband WSS Gaussian process. The spectrogram of sensor 1 of the experimental data in the 40- to 120-Hz band is shown in figure 16 and that of the simulated data in figure 17. We have retained the narrowband components in the simulated data. We notice in figure 17 the “bath tubbing” characteristic of a moving broadband source. CPA is clearly visible at approximately 35 minutes. The difference in the spectrograms of figures 16 and 17 is probably due to inaccurate environmental modeling, specifically in the sediment layer.

We believe these simulation results demonstrate the utility of this technique and that it will be useful in analyzing the effects of source movement on data analysis and signal processing algorithms.

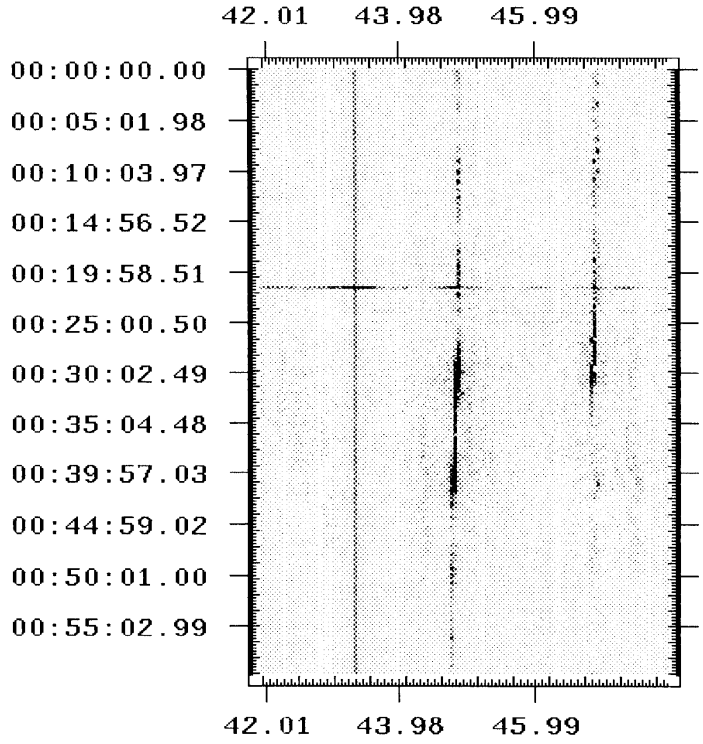


Figure 8. Experiment 45-Hz tonal on sensor 1.

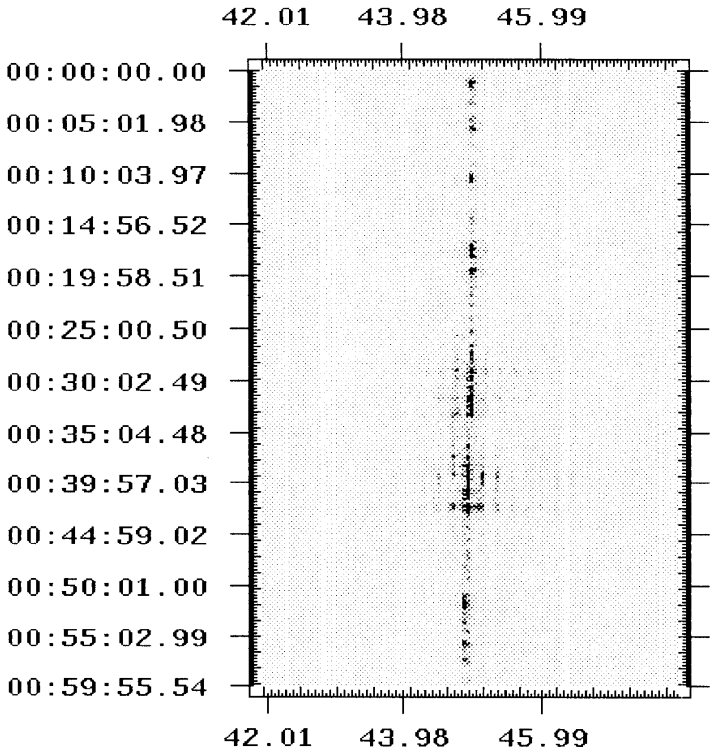


Figure 9. Simulation: 45-Hz tonal on sensor 1.

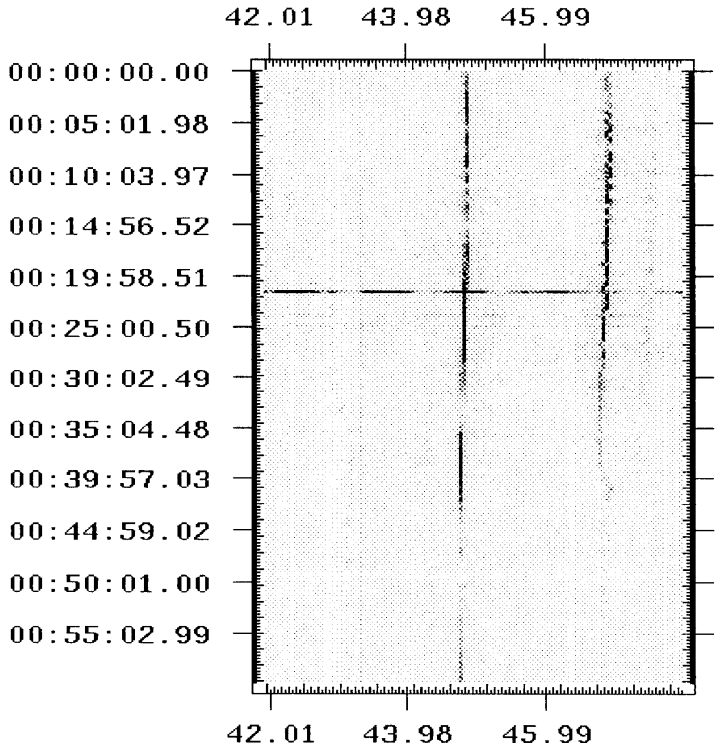


Figure 10. Experiment: 45-Hz tonal on sensor 2.

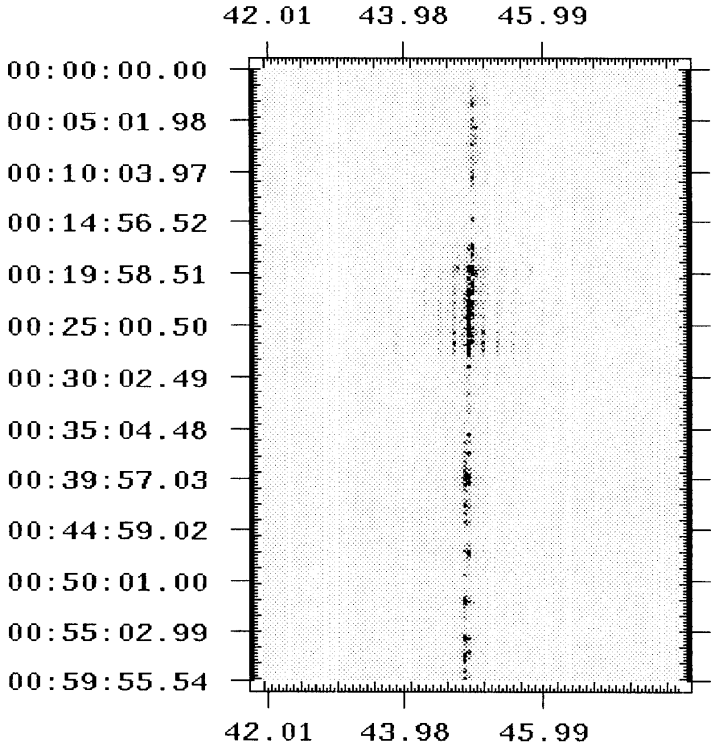


Figure 11. Simulation: 45-Hz tonal on sensor 2.

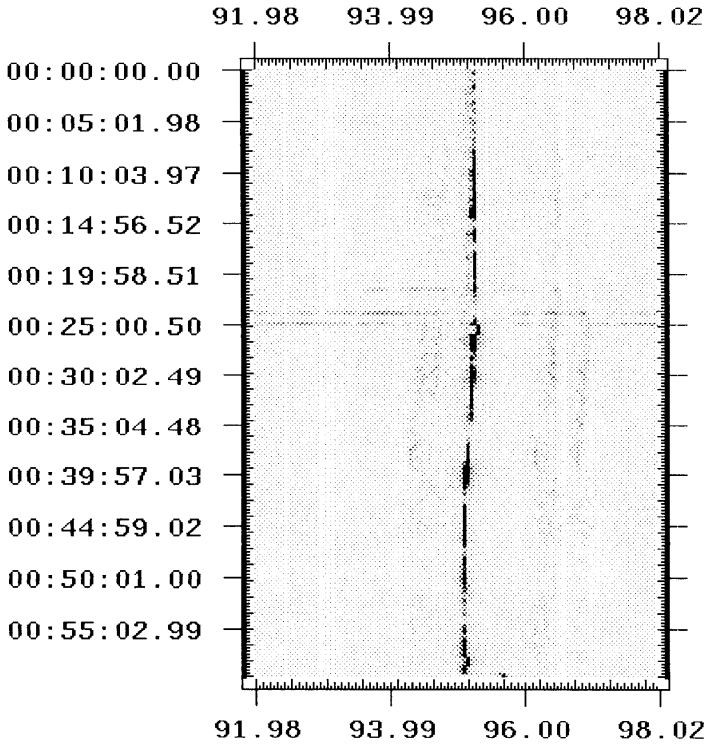


Figure 12. Experiment: 95-Hz tonal on sensor 1.

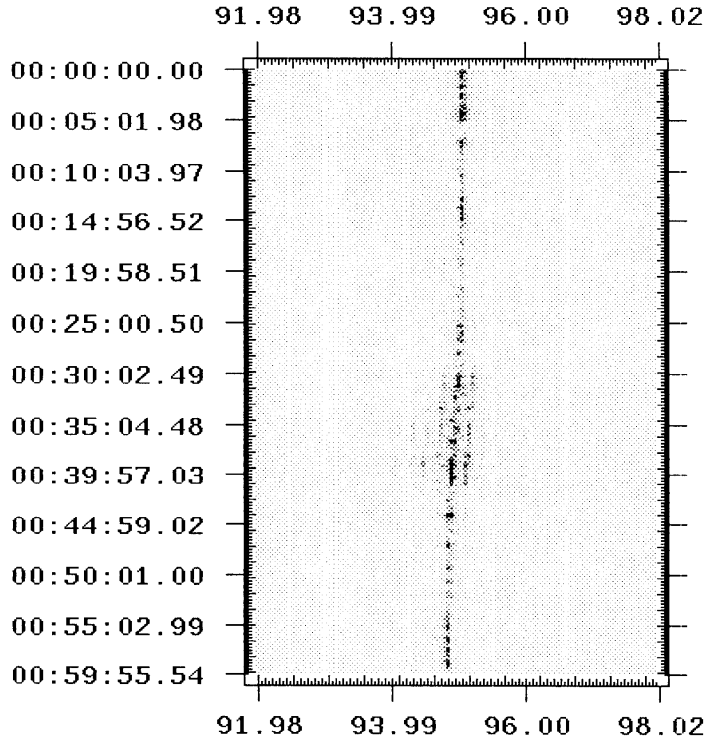


Figure 13. Simulation: 95-Hz tonal on sensor 1.

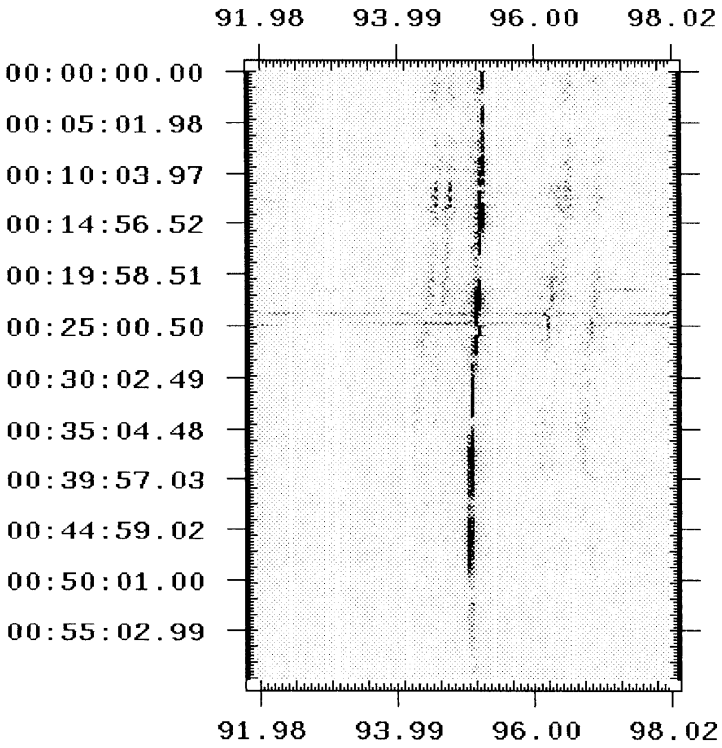


Figure 14. Experiment: 95-Hz tonal on sensor 2.

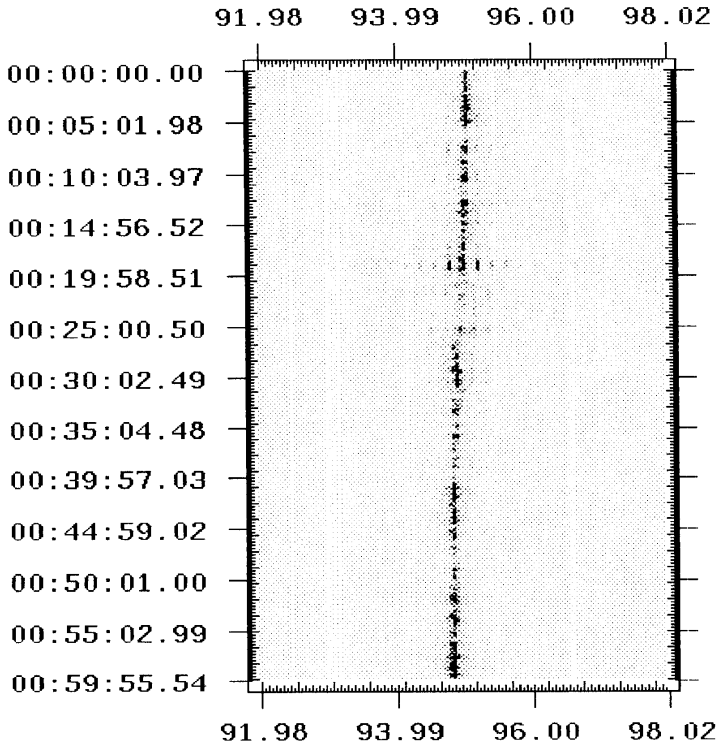


Figure 15. Simulation: 95-Hz tonal on sensor 2.

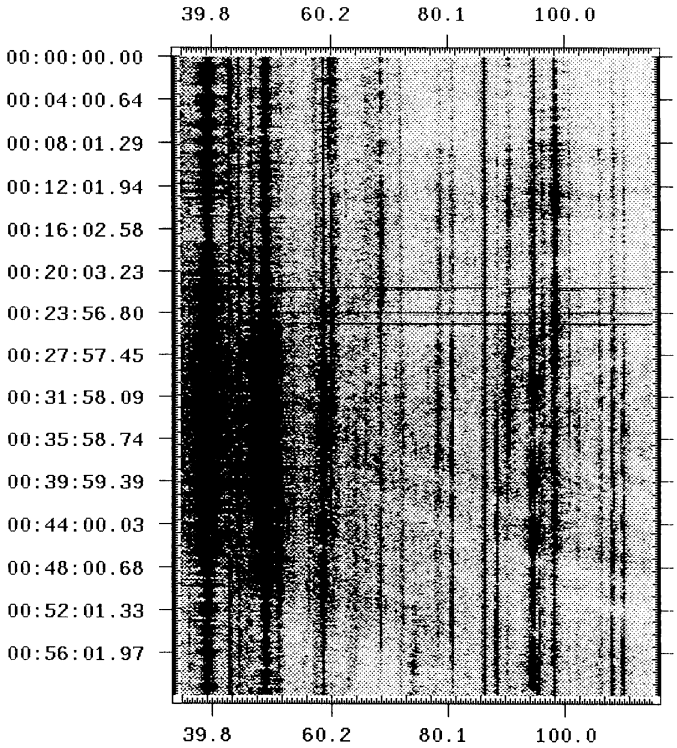


Figure 16. Experiment: 40- to 120-Hz band on sensor 1.

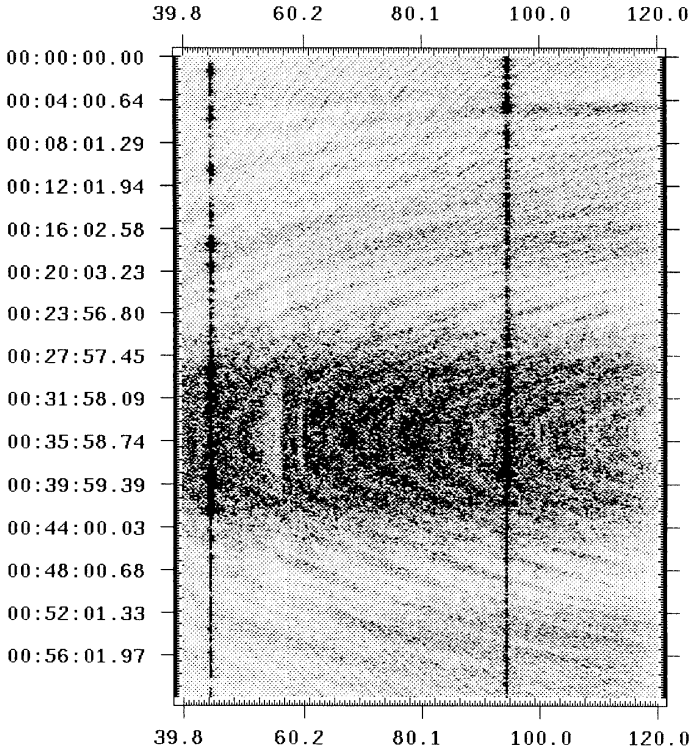


Figure 17. Simulation: 40- to 120-Hz band on sensor 1.

# 6 CONCLUSIONS

In this report, we demonstrate that the moving-source problem can be interpreted in terms of time-varying linear-systems theory. We then illustrate how we can use this interpretation to simulate the time series received at a sensor due to a moving source with arbitrary spectral characteristics. We show that simulated time series generated via this technique closely approximates experimental data. It is evident from this comparison that Doppler effects are correctly simulated.

The computational burden of this algorithm is directly related to the frequency sampling resolution and source bandwidth. The greater the dispersive nature of the channel, the finer the frequency resolution must be. So for complicated propagation environments, this algorithm can be quite computationally intensive due to the calculation of the bifrequency system function. Moreover, very broadband signals can also be computationally expensive to simulate.

# 7 RECOMMENDATIONS

The algorithm presented in this report is highly parallel in nature. The problem easily can be divided into independent spatial segments. Also, the calculation of the bifrequency system function can be implemented in terms of independent vector operations, which themselves can be efficiently executed on parallel or vector processors. So we believe the simulation could be effectively implemented on a highly parallel machine.

To simulate more realistic propagation environments, it may be necessary to extend the technique to account for three-dimensional propagation. While this would require initial analytical extensions to Hawker's results, the fundamental algorithm would not change.

We also recommend explicitly determining the spectral coherence function in terms of the acoustic parameters. This may lead to advanced array processing algorithms that use source motion as a target discriminant to enhance detection performance.

# 8 REFERENCES


[1] Brillinger, David R. 1981. *Time Series Data Analysis and Theory*, chapter 5. Holden–Day.

[2] Kay, Steven M. 1988. *Modern Spectral Estimation*, chapter 4. Prentice–Hall.

[3] Hawker, Kenneth E. 1979. "A normal mode theory of acoustic Doppler effects in the oceanic waveguide." *J. Acoust. Soc. Am.*, 65(3):675–681 (March).

[4] Rao, Kodali V., Thomas M. Michaud, and Henrik Schmidt. 1991. "Doppler shifts in underwater acoustics using field solutions." In *Oceans 91*, pp. 779–782.

[5] Song, Hee Chun, and A. B. Baggeroer. 1990. "The resolution of modal Doppler shifts in a dispersive oceanic waveguide." *J. Acoust. Soc. Am.*, 88(1):268–282 (July).

[6] Zala, Cedric A., and John M. Ozard. 1992. "Matched-field processing for a moving source." *J. Acoust. Soc. Am.*, 92(1):403–417 (July).

[7] Chen, Han-Yang, and I-Tai Lu. 1992. "Matched-mode processing schemes of a moving point source." *J. Acoust. Soc. Am.*, 92(4):2039–2050 (October).

[8] Zadeh, Lotfi A. 1950. "Frequency analysis of variable networks." *Proc. I.R.E.*, 38:291–299 (March).

[9] Huang, Nian-Chyi, and J. K. Aggarwal. 1980. "On linear shift-variant digital filters." *IEEE Trans. Circuits Syst.*, 27(8):672–679 (August).

[10] Saleh, Bahaa E. A., and Nikola S. Subotic. 1985. "Time-variant filtering of signals in the mixed time-frequency domain." *IEEE Trans. Acoust., Speech, Signal Processing*, 33(6):1479–1485 (December).

[11] Papoulis, Athanasios. 1985. *Probability, Random Variables, and Stochastic Processes*, chapter 10. McGraw-Hill.

[12] _____. 1962. *The Fourier Integral and Its Applications*, pp. 269–282. McGraw-Hill.

[13] McCann, Kevin J., and Freda Lee–McCann. 1991. "A narrow-band approximation to the acoustic pressure field." *J. Acoust. Soc. Am.*, 89(6):2670–2676 (June).

[14] Porter, Michael B. 1991. *The KRAKEN normal mode program*. SACLANT Undersea Research Centre, sm-245 edition.

# Appendix

## TIME-VARYING MODAL GROUP VELOCITY AND MODAL ARRIVAL TIME

In this appendix, we derive the modal group velocity and modal arrival time associated with the moving-source scenario described in sections 2 and 3.

We begin with the relationship between the time-varying channel impulse response and the system function described by equation 11:

$$h(t,\tau) = \frac{1}{2\pi}\int H(\omega;t)e^{-i\omega(\tau-t)}d\omega \tag{A-1}$$

We know from section 2 (equation 4) that the system function for the source–receiver scenario depicted in figure 1 can be approximated by

$$H(\omega;t) = \frac{-1}{\sqrt{8\pi}}e^{-i\pi/4}\sum_n \frac{Z_n(z_s)Z_n(z)}{\sqrt{k_nR_o}}\exp\left[-ik_nR_o\left(1-\frac{v}{v_n^g}\sin\theta_o\right)\right] \tag{A-2}$$

$$\exp\left[-iA_n(t-t_o)\right]e^{-\alpha_nR_o}$$

for $t_o + \mu_D - \frac{\Delta t}{2} < t < t_o + \mu_D + \frac{\Delta t}{2}$

where

$$A_n = k_nv\sin\theta_o - k_nv^2/v_n^g \tag{A-3}$$

Now, without loss of generality, we will assume that $t_o = 0$. $t_o$ trivially can be included at the end of the derivation. Next, let us define the phase of the integrand in equation A-1 to be

$$q = k_nR_o\left(1-\frac{v}{v_n^g}\sin\theta_o\right) + A_n(t) + \omega(\tau - t) \tag{A-4}$$

The modal group velocity occurs when we use the stationary phase technique to approximate the solution of equation A-1. Taking the derivative of $q$ with respect to $\omega$ and setting the result equal to zero, we get

$$\frac{\partial q}{\partial\omega} = \frac{R_o}{v_n^g}\left(1-\frac{v}{v_n^g}\sin\theta_o\right) + k_nR_o\frac{v}{(v_n^g)^2}\frac{\partial v_n^g}{\partial\omega}\sin\theta_o$$

$$-t\left[1-\frac{1}{v_n^g}\left(v\sin\theta_o - \frac{v^2}{v_n^g}\right) - k_n\left(\frac{v}{v_n^g}\right)^2\frac{\partial v_n^g}{\partial\omega}\right] + \tau = 0 \tag{A-5}$$

where we have used the fact that $v_n^g = \left(\frac{\partial k_n}{\partial \omega}\right)^{-1}$.

Next we solve the above equation for $t$ and label the solution $t_n$ to correspond to the $n^{\text{th}}$ mode. Now, intuitively we define the travel time or time delay of a mode as the difference between $t_n$ and the spatial time $\tau$, i.e., $M_{D,n} = t_n - \tau$. Using equation A-5, we get

$$M_{D,n} = \frac{\frac{R_o}{v_n^g}\left(1 - \frac{v}{v_n^g}\sin\theta_o E_n\right) + \tau\left[\frac{v}{v_n^g}\sin\theta_o - \left(\frac{v}{v_n^g}\right)^2 E_n\right]}{\left[1 - \frac{v}{v_n^g}\sin\theta_o + \left(\frac{v}{v_n^g}\right)^2 E_n\right]} \tag{A-6}$$

for $-\frac{\Delta t}{2} < \tau < \frac{\Delta t}{2}$, where

$$E_n = \left(1 - k_n \frac{\partial v_n^g}{\partial \omega}\right) \tag{A-7}$$

Now, we define the time-varying modal group velocity as $v_{n,\tau}^g = \frac{R_\tau}{(t_n - \tau)}$. Using the approximation of the time-varying range $R_\tau$ of section 2, i.e., $R_\tau \approx R_o + v\tau\sin\theta_o$, we get

$$v_{n,\tau}^g = \frac{\left(R_o + v\tau\sin\theta_o\right)\left[1 - \frac{v}{v_n^g}\sin\theta_o + \left(\frac{v}{v_n^g}\right)^2 E_n\right]}{\frac{R_o}{v_n^g}\left(1 - \frac{v}{v_n^g}\sin\theta_o E_n\right) + \tau\left[\frac{v}{v_n^g}\sin\theta_o - \left(\frac{v}{v_n^g}\right)^2 E_n\right]} \tag{A-8}$$

for $-\frac{\Delta t}{2} < \tau < \frac{\Delta t}{2}$.

Finally, a useful approximation of the modal travel time can be developed using the approximations $\frac{\partial v_n^g}{\partial \omega} \approx 0$, $E_n \approx 1$, and $\left(\frac{v}{v_n^g}\right)^2 \approx 0$. Then equation A-6 becomes

$$M_{D,n} \approx \frac{R_o}{v_n^g} + \tau\left(\frac{\frac{v}{v_n^g}\sin\theta_o}{1 - \frac{v}{v_n^g}\sin\theta_o}\right) \tag{A-9}$$

for $-\frac{\Delta t}{2} < \tau < \frac{\Delta t}{2}$.

To include nonzero $t_o$ in this analysis, we simply replace $\tau$ with $\tau - t_o$ in the above equations.